Ideal Discrete Energy Levels in Synthesized Au Nanoparticles for Chemically Assembled Single-Electron Transistors

Shinya Kano,[†,‡] Yasuo Azuma,[†,‡] Kosuke Maeda,[†,‡] Daisuke Tanaka,[‡,§] Masanori Sakamoto,[‡,⊥,∥] Toshiharu Teranishi,[‡,§,⊥] Luke W. Smith,[△] Charles G. Smith,[△] and Yutaka Majima[†,‡,#,*]

[†]Materials and Structures Laboratory, Tokyo Institute of Technology, Yokohama 226-8503, Japan, [‡]CREST, Japan Science and Technology Agency, Yokohama 226-8503, Japan, [§]Graduate School of Pure and Applied Sciences, University of Tsukuba, Tsukuba 305-8571, Japan, [⊥]Institute for Chemical Research, Kyoto University, Uji, Kyoto 611-0011 Japan, [∥]PRESTO, Japan Science and Technology Agency, Uji, Kyoto 611-0011 Japan, [△]Cavendish Laboratory, University of Cambridge, Cambridge CB3 0HE, U.K., and [#]Department of Printed Electronics Engineering, Sunchon National University, Sunchon 540-742, Korea

ABSTRACT Ideal discrete energy levels in synthesized Au nanoparticles (6.2 ± 0.8 nm) for a chemically assembled single-electron transistor (SET) are demonstrated at 300 mK. The spatial structure of the double-gate SET is determined by two gate and drain voltages dependence of the stability diagram, and electron transport to the Coulomb box of a single, nearby Coulomb island of Au nanoparticles is detected by the SET. The SET exhibits discrete energy levels, and the excited energy level spacing of the Coulomb island is evaluated as 0.73 meV, which well corresponds to the expected theoretical value. The discrete energy levels show magnetic field evolution with the Zeeman effect and dependence on the odd−even electron number of a single Au nanoparticle.

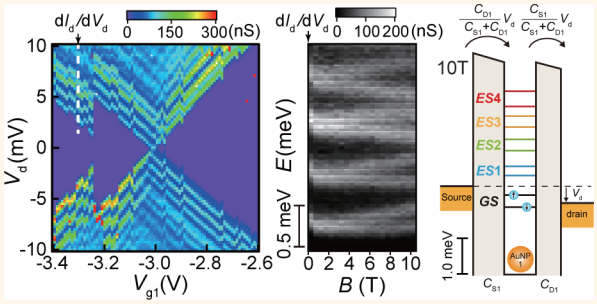

KEYWORDS: single-electron transistor · chemical assembly · Au nanoparticle · discrete energy level · Zeeman effect · parity

Chemical assembly is one of the promising candidates of fabrication processes for single-electron transistors (SETs). SETs are attractive components for high device density, high charge sensitivity, and low power consumption;[1−10] however, the reproducible fabrication of SETs is still a challenge. SETs consist of three (source, drain, and gate) electrodes, and a quantum dot as a Coulomb island has to be isolated by two tunneling junctions from source and drain electrodes. Semiconductors,[11−13] carbon nanomaterials,[14−16] single atoms,[17] and metallic nanoparticles (NP)[18−20] have been used as quantum dots, and their discrete energy level spectra have been demonstrated. Synthesized Au NPs have good features for Coulomb islands, since the size of the Au core can be controlled with a size distribution of ±10%,[21] and the tunneling resistances between the Au core and source/drain electrodes can be controlled by adjusting the length of the ligand shell molecule of the Au NPs.[22−24] Recently, we have developed fabrication techniques for robust nanogap electrodes with a separation of 3.0 ± 1.7 nm in a yield of 90% by electroless gold plating. Our nanogap electrodes maintain both their structure unchanged up to temperatures of 170 °C during the isotropic oxygen plasma process and their surface reactivity to form a self-assembled monolayer.[25,26] We have fabricated chemically assembled SETs that consist of synthesized Au NPs, electroless gold-plated nanogap electrodes, and an anchor molecule of alkanedithiol mixed with alkanethiol self-assembled monolayers (SAMs), and demonstrated ideal rhombic Coulomb diamonds and all two-input gates logic operations on chemically assembled SETs.[7−10]

Here, we show that the application of synthesized Au NP quantum dots to chemically assembled SET provides ideal discrete energy levels; the SET is able to detect single

* Address correspondence to majima@msl.titech.ac.jp.

Received for review August 8, 2012 and accepted October 19, 2012.

Published online October 19, 2012
10.1021/nn303585g

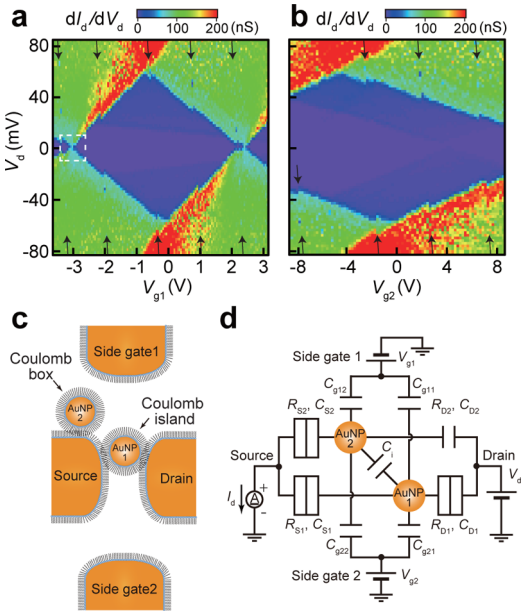

Figure 1. (a, b) Stability diagram of dI_d/dV_d as a function of V_d and (a) V_{g1} and (b) V_{g2} at 300 mK. Pairs of arrows indicate the abrupt shift lines of the Coulomb diamond resulting from a Q_0 change by the transition of a single electron to Au NP2. Stability diagrams taken from the areas indicated by the dashed white line are presented in Figure 2a. (c) Schematic of the spatial structure of the chemically assembled SETs consisting of electroless gold-plated electrodes and two Au NPs. (d) The equivalent SET circuit. The resistances and capacitances R_{Sk} and C_{Sk} are those of Au NPk (k = 1 or 2) at source side junction, R_{Dk} and C_{Dk} are those of Au NPk (k = 1 or 2) at the drain side junction, and C_{gjk} is a side gate capacitance between side gate j and Au NPk. The interdot capacitance between Au NP1 and Au NP2 is C_i.

electron transport to the Coulomb box near the Au NP. Two gate and drain voltages dependence of the stability diagrams determine the spatial structure of the Au NPs and nanogap electrodes, and we discuss the discrete energy level spacing of a single Au NP, the Zeeman splitting of the magnetic field evolution of the discrete energy level spectra, and the odd–even electron number dependence of Zeeman splitting.

RESULTS AND DISCUSSION

Figure 1a and b show the stability diagrams of the differential conductance of the drain current (dI_d/dV_d) of the double-gate SET as a function of the side gate voltages (V_{g1} and V_{g2}) and V_d. Clear Coulomb diamonds are observed in Figure 1a and b. The shape of Coulomb diamonds is an ideal rhombic shape, which corresponds to characteristics of SET with a single quantum dot; therefore a single Au NP (Au NP1) is attributed to the Coulomb diamond characteristics.[2,9,10] As the two-dimentional current–voltage characteristics of the stability diagrams in Figure 1a and 1b are very stable, all of the SET circuit parameters can be evaluated by fitting theoretical Coulomb diamonds and Coulomb blockade behavior with the experimental results;[9,10,22,23,27,28] the capacitance parameters

TABLE 1. SET Circuit Parameters for the Circuit in Figure 1d[a]

k	R_{Sk}	C_{Sk}	R_{Dk}	C_{Dk}	C_{g1k}	C_{g2k}
Au NP1	4.8 MΩ	1.25 aF	1.5 MΩ	1.58 aF	31.5 zF	5.2 zF
Au NP2		≈1.3 aF		0.25 aF	120 zF	36 zF

[a] All parameters are evaluated using orthodox theory or the gate modulation period. C_i = 53 zF.

between Au NP1 and the source electrode (C_{S1}), drain electrode (C_{D1}), side gate 1 electrode (C_{g11}), and side gate 2 electrode (C_{g21}) can be determined from the slope of the Coulomb diamond thresholds in Figure 1a and 1b. In contrast, the SET resistance parameters between Au NP1 and the source electrode (R_{S1}) and drain electrode (R_{D1}) can be determined from the Coulomb blockade in Figure S1c. The evaluated parameters are listed in Table 1, and the theoretical stability diagram shows good agreement with those in Figure 1a and 1b (see Supporting Information).

In Figure 1a and b, there are pairs of arrows indicating abrupt shifts along the V_d axis in the Coulomb diamond, and these shifts can be attributed to the detection of discrete single-electron transport by the double-gate SET.[29] Because single-electron transports are also periodically modulated by the gate voltages of V_{g1} and V_{g2}, the origin of the charge transport is explained by the existence of another single Au NP (Au NP2) chemisorbed onto the source electrode as a Coulomb box as follows: The single-electron transport periods of ΔV_{g1} (= 1.3 V) and ΔV_{g2} (= 4.5 V) give the gate capacitances of Au NP2 (C_{g12} and C_{g22}) as 120 and 36 zF, respectively. The slopes of the boundary of the single-electron transport (indicated by pairs of arrows) correspond to the ratios of the drain voltage and the gate voltage and are evaluated as $\Delta V_d/\Delta V_{g1}$ = 0.47 and $\Delta V_d/\Delta V_{g2}$ = 0.14, respectively. The capacitance between Au NP2 and the drain electrode (C_{D2}) is given from these slopes as $C_{D2} = C_{gk2}\Delta V_{gk}/\Delta V_d$ (k = 1 and 2), and the values of C_{D2} are evaluated as 0.25 aF by $C_{g12}\Delta V_{g1}/\Delta V_d$ and 0.25 aF by $C_{g22}\Delta V_{g2}/\Delta V_d$, respectively. It is noted that the same values of C_{D2} (= 0.25 aF) are evaluated from different Coulomb diamonds oscillated by V_{g1} and V_{g2}. C_{D2} is 6 times smaller than the capacitance between the chemisorbed Au NP and the electrode, *i.e.*, C_{D1}. Therefore, Au NP2 chemisorbed onto only the source electrode and was capacitively coupled to the drain electrode. The abrupt shifts in V_{g1} and V_{g2} are evaluated as 0.15 and 0.80 V from Figure 1a and b, respectively, which correspond to fractional residual charge (Q_0) shifts of 0.03e and 0.03e by comparison with the Coulomb diamond period, respectively, where e is the unit charge. The internal capacitance between Au NP1 and Au NP2 (C_i) is evaluated to be 53 zF from $eC_i/(C_{S2} + C_{D2} + C_{g12} + C_{g22} + C_i)$ = 0.03e if the capacitance between Au NP2 and the source electrode (C_{S2}) is assumed to be 1.3 aF,

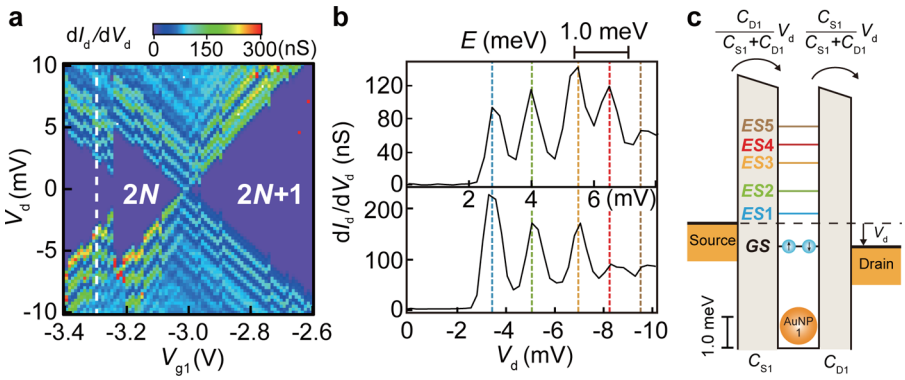

Figure 2. (a) Stability diagram of dI_d/dV_d as a function of V_d and V_{g1} at the double-degeneracy points in the Coulomb diamond indicated by the dashed white boxes in Figure 1a. Each satellite line is attributed to the excited states (ES) of Au NP1. The number of electrons in each Coulomb diamond is shown in the plots. Each discrete energy state has two spin-degenerate electrons, and if the states lower than the ground state (GS) are fully occupied, the number of electrons is 2*N*. (b) Line profiles of dI_d/dV_d-V_d in the (c) positive V_d regions taken along the dashed lines in (a). Each peak is attributed to an excited energy level of Au NP1. (c) Schematic energy diagram of the excited energy levels of Au NP1 under a magnetic field of $B = 0$ T.

which is similar to the capacitance between the chemisorbed Au NP and the electrode, *i.e.*, C_{S1}.

It is noted that another Coulomb diamond, 20 times less conductive than the main Coulomb diamonds, are superimposed in Figure 1a and 1b, and this result implies another Au NP (Au NP3 named in Supporting Information) is inserted in parallel with Au NP1. As the effect of Au NP3 is negligibly small, the SET can be considered as an SET consisting of Au NP1 as the Coulomb island and Au NP2 as the Coulomb box near Au NP1, which is similar to the other experimental results and theoretical proposals.[3−10] A detailed discussion about Au NP3 is in the Supporting Information. Consequently, the schematic spatial structure of the Au NPs and nanogap electrodes in this double-gate SET and the equivalent circuit are shown in Figure 1c and d, respectively, and the unique circuit parameters are evaluated as discussed above and listed in Table 1 (a scanning electron microscopy image of typical electroless gold-plated nanogap electrodes is shown in Supporting Information Figure S2).

Differential conductance peaks appear as satellite lines parallel to the Coulomb diamond edges, and they originate from the transmission resonances of the excited levels in the Coulomb island aligned with the Fermi levels of the source or drain electrodes.[12,20] Figure 2a shows the discrete energy level spectra of Au NP1 at the degeneracy points of two Coulomb diamonds. Multiple parallel bright lines with both positive and negative slopes correspond to the transmission resonance through excited levels from the drain and source electrode, respectively. We note that the right-hand side slope of the Coulomb diamond corresponds to electron transfer into unoccupied states and that the left-hand side slope corresponds to electron transfer out of the occupied states. The obtained differential conductance of the drain current−drain voltage (dI_d/dV_d-V_d) characteristics was converted into the electronic energy potential of the Coulomb island by considering the capacitive division of the voltage across two tunneling junctions.[18−20]

The voltages across junction 1 (V_1), consisting of R_{S1} and C_{S1}, and across junction 2 (V_2), consisting of R_{D1} and C_{D1}, are

$$V_1 = \frac{C_{D1}}{C_{S1}+C_{D1}}V_d \quad (1)$$

$$V_2 = \frac{C_{S1}}{C_{S1}+C_{D1}}V_d \quad (2)$$

from Kirchhoff's voltage law, where C_{g11} and C_{g21} are negligibly smaller than C_{S1} and C_{D1}. The voltage difference in eqs 1 and 2 is equal to the electronic energy potential shift of the Coulomb island.

Figure 2b shows dI_d/dV_d-V_d characteristics taken along the dashed lines in Figure 2a, respectively. Each dI_d/dV_d peak corresponds to tunneling of the electron through the excited energy states of a Au NP. The positive and negative bias spectra show good agreement with each other after considering the capacitive division, and the conductance peak heights correspond to the tunneling rates in each tunneling junction. A schematic energy diagram of each NP is shown in Figure 2c, and each dI_d-dV_d peak in Figure 2b corresponds to one of these excited energy states (indicated by the colored dashed lines). From the spectra in Figure 2b, the mean excited level spacing of Au NP1 is evaluated to be $\Delta E = 0.73$ meV.

The expected mean excited level spacing of spin-degenerate energy levels can be predicted by

$$\Delta E \approx \frac{2\pi^2\hbar^2}{m_e k_F V} \quad (3)$$

where $\hbar$ is the Planck constant, m_e is the electron mass, and k_F is the Fermi wave vector (1.21×10^{10} m^{-1} for Au).[18,30] Assuming a single Au NP is spherical in shape, the NP volume can be evaluated by $V = 4\pi r^3/3$, where r is the radius. For an average diameter of 6.2 ± 0.8 nm,

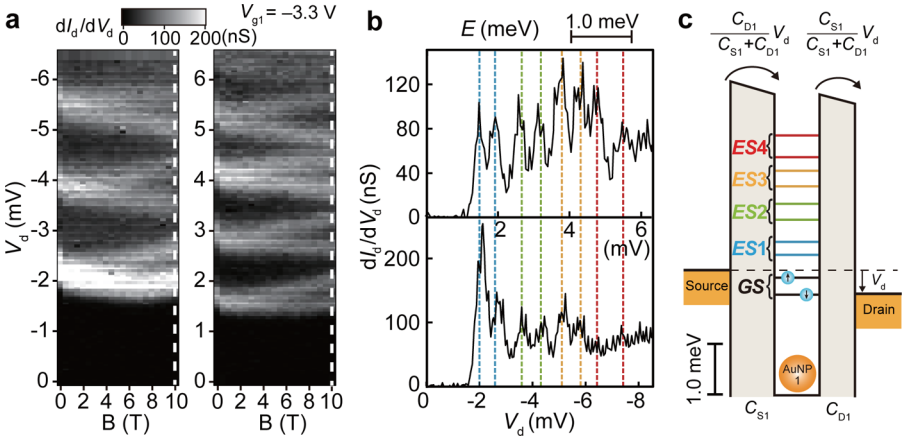

Figure 3. (a) Magnetic field evolution of the dI_d/dV_d peaks at $V_{g1} = -3.3$ V. The white areas show larger dI_d/dV_d values. (b) Line profiles taken along the dashed lines indicated in part (a) of $dI_d/dV_d - V_d$ in the positive and negative V_d regions under a magnetic field of $B = 10$ T. Each peak is attributed to the splitting of the excited energy levels of Au NP1. (c) Schematic energy diagram of the excited energy levels of Au NP1 under a magnetic field of $B = 10$ T.

ΔE should be in the range 0.7−1.5 meV . Individual levels of a 6.2 nm Au NP should be resolvable considering $\Delta E \geq 3.5k_BT = 0.09$ meV at 300 mK.[18] Therefore, the experimental ΔE values are consistent with that derived for a Au NP diameter of 6.2 ± 0.8 nm from eq 3. As the values of C_{S1} and C_{D1} are determined as 1.25 and 1.58 aF with the accuracy of 0.01 aF, respectively, the energy level spacing can be evaluated with an accuracy of 0.01 meV by eqs 1 and 2.

Kuemmeth *et al.*[20] have reported discrete energy level spectra of synthesized Au NPs (core diameter of 5−15 nm) with electromigrated nanogap electrodes. Compared to their reports, the discrete energy level spectra in our SETs are more uniformly distributed, and the distribution along the V_d axis can be fully explained using the junction parameters in Table 1. These ideal characteristics can be attributed to the electroless gold-plated nanogap electrodes for which the nanogap separation and shape are precisely controlled (Supporting Information Figure S2), because the SET characteristics strongly depend on the electrode structure.

The spin state of the electrons in Au NP1 are discussed as follows: As has been previously reported, the electron energy levels exhibit 2-fold Kramers degeneracy at zero magnetic field B with respect to the spin quantum number, and the 2-fold energy level splits as B is increased (the Zeeman effect).[18−20] Figure 3a shows the magnetic field dependence of dI_d/dV_d as a function V_d for $V_{g1} = -3.3$ V. Larger dI_d/dV_d values are represented in white. (The I_d and dI_d/dV_d characteristics at $B = 0$ T and $B = 10$ T are shown in Supporting Information Figure S3.) Splitting of the excited energy states can be observed in the figures, and the evolution in both the positive and negative V_d regions shows similar behavior. Line profiles along the dotted lines in Figure 3a are shown in Figure 3b. After placing the results on an energy scale, this figure supports the hypothesis that electrons are transferred through the same Au NP excited states in both the positive and negative V_d regions. A schematic energy diagram of the Au NP at $B = 10$ T is shown in Figure 3c.

We can estimate the g-factor for the electron in the Au NPs from the Zeeman effect. The relationship between the g-factor and the energy difference of two split levels δE is $\delta E = g\mu_B B$, where μ_B is the Bohr magneton. From Figure 3b, δE is evaluated to be 0.33 meV at $B = 10$ T, giving a g-factor of 0.57, which agrees well with previous reports.[20] The value is less than 2.0 because of the strong spin−orbit interaction in the Au atoms.[19]

The number of electrons confined to the Coulomb island is different for each adjacent Coulomb diamond by exactly one electron, as shown in Figure 4a, where $2N$ is the number of electrons on the SET. When the charge configuration of the SET moves from electron number $2N$ to $2N + 1$, the lowest excited energy state of the Coulomb island is filled with one electron transferred from the electrode, and that filled state will no longer be available for an electron tunneling transition.[12,18,19] Figure 4b−d show the magnetic field evolution of the excited energy states in a positive V_d region under V_{g1} values of −3.3, 1.9, and 7.3 V. (The evolution in the negative V_d region is also shown in Supporting Information Figure S4b−d.) The lowest excited energy state disappears as the number of electrons on Au NP1 increases, which means that one electron is transferred and filling of the lowest excited energy state proceeds in line with an increase in V_{g1}. The spectra for each V_{g1} show identical magnetic field evolution, and clear identification of the three consecutive charge configurations is attributed to the odd−even electron number of a single Au NP. Therefore, the chemically synthesized double-gate SET consisting of electroless gold-plated nanogap electrodes and

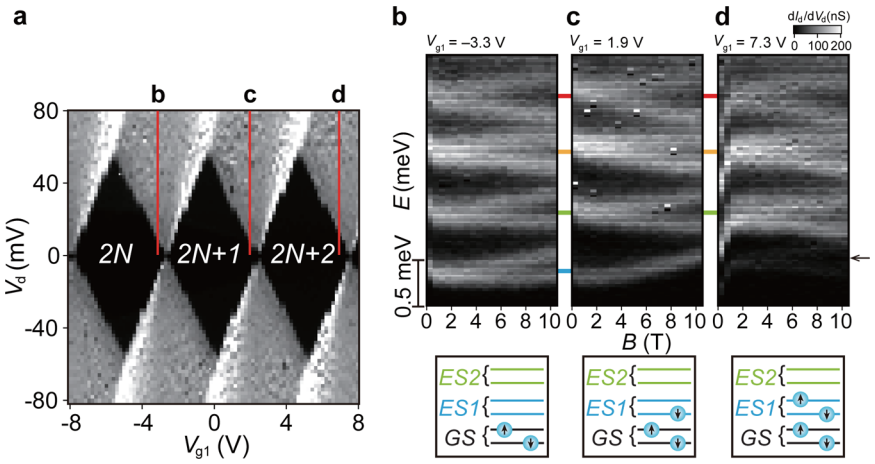

Figure 4. (a) Relationship between the electron number and Coulomb diamonds, as in Figure 1a. (b–d) Line profiles taken from part (a) of the magnetic field evolution of the dI_d/dV_d peaks at V_{g1} values of (b) −3.3 V, (c) 1.9 V, and (d) 7.3 V in the positive V_d region. The electron configuration in the excited energy levels of Au NP1 is shown below each plot. The arrow in (d) indicates the splitting of the energy levels of Au NP3 near Au NP1.

synthesized Au NP is a good platform to observe ideal and reproducible SET characteristics.

CONCLUSION

In conclusion, we have demonstrated the discrete energy level spectra of synthesized Au NPs with electroless gold-plated nanogap electrodes in a chemically assembled SET. The spatial structure of the Au NPs and nanogap electrodes was uniquely determined by two gate voltages dependence of the stability diagrams. The SETs show an ideal rhombic Coulomb diamond with satellite lines originating from the excited energy levels of the Au NPs. The magnetic field evolution of the discrete energy level spectra showed the Zeeman effect and dependence on the odd–even electron number in the Au NP. The fabricated SETs also work as charge sensors for detecting electron transport to the Coulomb box near the Au NP. These results are significant for the realization of single-electron sensing devices, since chemically assembled SETs have strong advantages such as air stability, well-controlled electrical characteristics, simultaneous fabrication, and ideal discrete energy levels.

METHODS

Chemically assembled SETs with double-side-gate structure identical to our previous reports[7,9,10] were assembled for this study using Au NP quantum dots. The Au NPs were chemically synthesized using established methods[21] and had core diameters and a standard deviation of 6.2 ± 0.8 nm, as estimated from transmission electron microscopy (TEM) images (Supporting Information Figure S6). The Au NPs were stabilized by decanethiol ligand molecules.

Stable SETs functionalized with self-assembled monolayers and Au NPs were simultaneously fabricated by a combination of top-down and chemical bottom-up techniques. Electroless gold-plated nanogap electrodes were used, as the size can be controlled so that it is suitable for the Au NPs,[25,26] and the SAMs were formed in such a way that the chemically assembled SETs are stable even under ambient conditions.[10] The SET fabrication method we employed enabled us to prepare multiple chemically assembled SETs at the same time.

We measured the drain current–drain voltage (I_d–V_d) and drain current–gate voltage (I_d–V_g) characteristics of the SETs at 300 mK and calculated the differential conductance of the drain current–drain voltage (dI_d/dV_d–V_d) characteristics by numerically differentiating the I_d–V_d curve directly without lock-in amplifiers.

Conflict of Interest: The authors declare no competing financial interest.

Acknowledgment. This study was partially supported by a Grant-in-Aid for Scientific Research on Innovative Areas (No. 20108011, π-Space) from the Ministry of Education, Culture, Sports, Science and Technology (MEXT); MEXT Elements Strategy Initiative to Form Core Research Center; a Grant-in-Aid for Scientific Research (A) (23245028) from MEXT (T.T.); a Grant-in-Aid for Japan Society for the Promotion of Science (JSPS) Fellows (No. 11J08966) from MEXT (S.K.); a research grant from The Murata Science Foundation (Y.A.); the Collaborative Research Project of Materials and Structures Laboratory, Tokyo Institute of Technology; the Collaborative Research Program of the Institute for Chemical Research, Kyoto University (Grant 2012-63); and the World Class University (WCU) Program through the Ministry of Education, Science and Technology of Korea (R31-10022).

Supporting Information Available: Figures S1–S9, sample preparation technique, details of measurement procedure, and existence of another Au NP near Au NP1. This material is available free of charge *via* the Internet at http://pubs.acs.org.

REFERENCES AND NOTES

1. Likharev, K. K. Single-Electron Devices and Their Applications. *Proc. IEEE* **1999**, *87*, 606–632.
2. Durrani, Z. A. K. *Single-Electron Devices and Circuits in Silicon*; Imperial College: London, 2009; Chapter 2.
3. Chaki, N. K.; Singh, P.; Dharmadhikari, C. V.; Vijayamohanan, K. P. Single-Electron Charging Features of Larger, Dodecanethiol-Protected Gold Nanoclusters: Electrochemical and Scanning Tunneling Microscopy Studies. *Langmuir* **2004**, *20*, 10208–10217.

4. Luo, K.; Chae, D.-H.; Yao, Z. Room-Temperature Single-Electron Transistors Using Alkanedithiols. *Nanotechnology* **2007**, *18*, 465203.
5. Cervera, J.; Mafé, S. Multivalued and Reversible Logic Gates Implemented with Metallic Nanoparticles and Organic Ligands. *ChemPhysChem* **2010**, *11*, 1654–1658.
6. Cervera, J.; Mafé, S. Information Processing Schemes Based on Monolayer Protected Metallic Nanoclusters. *J. Nanosci. Nanotechnol.* **2011**, *11*, 7537–7548.
7. Azuma, Y.; Yasutake, Y.; Kono, K.; Kanehara, M.; Teranishi, T.; Majima, Y. Single-Electron Transistor Fabricated by Two Bottom-up Processes of Electroless Au Plating and Chemisorption of Au Nanoparticle. *Jpn. J. Appl. Phys.* **2010**, *49*, 090206.
8. Azuma, Y.; Suzuki, S.; Maeda, K.; Okabayashi, N.; Tanaka, D.; Sakamoto, M.; Teranishi, T.; Buitelaar, M. R.; Smith, C. G.; Majima, Y. Nanoparticle Single-Electron Transistor with Metal-Bridged Top-Gate and Nanogap Electrodes. *Appl. Phys. Lett.* **2011**, *99*, 073109.
9. Okabayashi, N.; Maeda, K.; Muraki, T.; Tanaka, D.; Sakamoto, M.; Teranishi, T.; Majima, Y. Uniform Charging Energy of Single-Electron Transistors by Using Size-Controlled Au Nanoparticles. *Appl. Phys. Lett.* **2012**, *100*, 033101.
10. Maeda, K.; Okabayashi, N.; Kano, S.; Takeshita, S.; Tanaka, D.; Sakamoto, M.; Teranishi, T.; Majima, Y. Logic Operations of Chemically Assembled Single-Electron Transistor. *ACS Nano* **2012**, *6*, 2798–2803.
11. Tarucha, S.; Austing, D. G.; Honda, T.; van der Hage, R. J.; Kouwenhoven, L. P. Shell Filling and Spin Effects in a Few Electron Quantum Dot. *Phys. Rev. Lett.* **1996**, *77*, 3613–3616.
12. Stewart, D. R.; Sprinzak, D.; Marcus, C. M.; Duruöz, C. I.; Harris, J. S., Jr. Correlations Between Ground and Excited State Spectra of a Quantum Dot. *Science* **1997**, *278*, 1784–1788.
13. Sasaki, S.; Franceschi, S. D.; Elzerman, J. M.; van der Wiel, W. G.; Eto, M.; Tarucha, S.; Kouwenhoven, L. P. Kondo Effect in an Integer-Spin Quantum Dot. *Nature* **2000**, *405*, 764–767.
14. Cobden, D. H.; Bockrath, M.; McEuen, P. L; Rinzler, A. G.; Smalley, R. E. Spin Splitting and Even-Odd Effects in Carbon Nanotubes. *Phys. Rev. Lett.* **1998**, *81*, 681–684.
15. Park, H.; Park, J.; Lim, A. K. L.; Anderson, E. H.; Alivisatos, A. P.; McEuen, P. L. Nanomechanical Oscillations in a Single-C_{60} Transistor. *Nature* **2000**, *407*, 57–60.
16. Moriyama, S.; Fuse, T.; Suzuki, M.; Aoyagi, Y.; Ishibashi, K. Four-Electron Shell Structures and an Interacting Two-Electron System in Carbon-Nanotube Quantum Dots. *Phys. Rev. Lett.* **2005**, *94*, 186806.
17. Fuechsle, M.; Miwa, J. A.; Mahapatra, S.; Ryu, H.; Lee, S.; Warschkow, O.; Hollenberg, L. C. L.; Klimeck, G.; Simmons, M. Y. A Single-Atom Transistor. *Nat. Nanotechnol.* **2012**, *7*, 242–246.
18. Ralph, D. C.; Black, C. T.; Tinkham, M. Spectroscopic Measurements of Discrete Electronic States in Single Metal Particles. *Phys. Rev. Lett.* **1995**, *74*, 3241–3244.
19. Petta, J. R.; Ralph, D. C. Studies of Spin-Orbit Scattering in Noble-Metal Nanoparticles Using Energy-Level Tunneling Spectroscopy. *Phys. Rev. Lett.* **2001**, *87*, 266801.
20. Kuemmeth, F.; Bolotin, K. I.; Shi, S.-F.; Ralph, D. C. Measurement of Discrete Energy-Level Spectra in Individual Chemically Synthesized Gold Nanoparticles. *Nano Lett.* **2008**, *8*, 4506–4512.
21. Teranishi, T.; Hasegawa, S.; Shimizu, T.; Miyake, M. Heat-Induced Size Evolution of Gold Nanoparticles in the Solid State. *Adv. Mater.* **2001**, *13*, 1699–1701.
22. Zhang, H.; Yasutake, Y.; Shichibu, Y.; Teranishi, T.; Majima, Y. Tunneling Resistance of Double-Barrier Tunneling Structures with an Alkanethiol-Protected Au Nanoparticle. *Phys. Rev. B* **2005**, *72*, 205441.
23. Kano, S.; Azuma, Y.; Kanehara, M.; Teranishi, T.; Majima, Y. Room-Temperature Coulomb Blockade from Chemically Synthesized Au Nanoparticles Stabilized by Acid-Base Interaction. *Appl. Phys. Express* **2010**, *3*, 105003.
24. Koo, H.; Kano, S.; Tanaka, D.; Sakamoto, M.; Teranishi, T.; Cho, G.; Majima, Y. Characterization of Thiol-Functionalized Oligo(phenylene-ethynylene)-Protected Au Nanoparticle by Scanning Tunneling Microscopy and Spectroscopy. *Appl. Phys. Lett.* **2012**, *101*, 083115.
25. Yasutake, Y.; Kono, K.; Kanehara, M.; Teranishi, T.; Buitelaar, M. R.; Smith, C. G.; Majima, Y. Simultaneous Fabrication of Nanogap Gold Electrodes by Electroless Gold Plating Using a Common Medical Liquid. *Appl. Phys. Lett.* **2007**, *91*, 203107.
26. Serdio V., V. M.; Azuma, Y.; Takeshita, S.; Muraki, T.; Teranishi, T.; Majima, Y. Robust Nanogap Electrodes by Self-terminating Electroless Gold Plating. *Nanoscale*, in press, DOI: 10.1039/C2NR32232C
27. Hanna, A. E.; Tinkham, M. Variation of the Coulomb Staircase in a Two-Junction System by Fractional Electron Charge. *Phys. Rev. B* **1991**, *44*, 5919–5922.
28. Li, X.; Yasutake, Y.; Kono, K.; Kanehara, M.; Teranishi, T.; Majima, Y. Au Nanoparticles Chemisorbed by Dithiol Molecules Inserted in Alkanethiol Self-Assembled Monolayers Characterized by Scanning Tunneling Microscopy. *Jpn. J. Appl. Phys.* **2009**, *48*, 04C180.
29. Mahapatra, S.; Büch, H.; Simmons, M. Y. Charge Sensing of Precisely Positioned P Donors in Si. *Nano Lett.* **2011**, *11*, 4376–4381.
30. Ashcroft, N. W.; Mermin, N. D. *Solid State Physics*; Brooks/Cole: Pacific Grove, 1976; p 38.